Desalination and Water Treatment
www.deswater.com
doi: 10.5004/dwt.2023.29835

305 (2023) 201–216
September

Kinetics and adsorption isotherm studies of Methylene blue and Direct red 81 onto post-coagulation sludge

Barbara Pieczykolan[a,*], Barbara Solecka[b]

[a]*Department of Water and Wastewater Engineering, Faculty of Energy and Environmental Engineering, The Silesian University of Technology, Konarskiego 18, 44–100 Gliwice, Poland, email: barbara.pieczykolan@polsl.pl*
[b]*Institute of Physics – Centre for Science and Education, Division of Applied Physics, The Silesian University of Technology, Konarskiego 22B, 44–100 Gliwice, Poland, email: barbara.solecka@polsl.pl*

Received 30 January 2023; Accepted 10 August 2023

ABSTRACT

Water treatment residuals generated during coagulation/flocculation, called also post-coagulation sludge, were used as adsorbents for Methylene blue (MB) and Direct red 81 (DR 81) adsorption. The adsorbent was characterized by specific surface area, scanning electron microscope, and Fourier-transform infrared spectroscopy measurement. Moreover, to characterize the adsorbent surface, the novelty approach of impedance measurement was applied in the studies. The Brunauer–Emmett–Teller of the sludge was 142.8651 m^2/g. Moreover, the impedance studies showed a significant change in the normalized real component of the impedance after the adsorption process. For MB this dye deteriorates the electrical properties of the adsorbent surface, while DR 81 improves them. The batch adsorption experiments were conducted as a function of pH value, contact time, and initial concentration of the dyes. The results showed that the adsorption effectiveness of DR 81 radically decreased at higher pH than 2, while the efficiency of MB adsorption was increasing as the value of pH increased, and the highest uptake of MB was for pH 10. The required contact time for MB was 30 min whereas for DR 81 it was longer and equalled 90 min. The adsorption kinetics followed the Elovich and pseudo-second-order model for both dyes. That indicates the rate-limiting step involves the chemisorption. A much higher adsorption rate was obtained for MB than for DR 81. The equilibrium experiment result showed that the obtained data were well represented by the Jovanovic and Sips isotherm models. The maximum adsorption capacity according to the Jovanovic isotherm model was similar for both dyes and was equalled 871.6 and 823.1 mg/g for DR 81 and MB, respectively. Based on obtained results, it can be concluded that the water treatment residuals can be effectively used as adsorbent for MB and DR 81 removal from aqueous solutions.

Keywords: Synthetic dye; Adsorption; Water treatment residuals; Adsorption kinetics; Adsorption isotherm

1. Introduction

Different types of dyes are used in all the production processes of such products as paints, clothes, colorful interior decorations, colorful panoramic photos decorating smaller or larger flat surfaces, for example, walls, but also cosmetics, food products, medicines, etc. As a result, of those production actions, wastewater is also generated that contains residues of dyes not used in production processes. It is obvious that wastewater containing dyes cannot be discharged directly into the environment. The need to treat this type of wastewater is supported by many aspects related to the protection of human health and life as well as environmental protection. Dyes constitute an extremely wide range of chemical compounds, among which there may also be toxic compounds (dyes containing heavy metals or aromatic

* Corresponding author.

Presented at the 3rd International Conference on Strategies toward Green Deal Implementation – Water, Raw Materials and Energy (ICGreenDeal2022), 5–7 December 2022, held online by the Mineral and Energy Economy Research Institute, Polish Academy of Sciences

1944-3994/1944-3986

compounds), but also cancerogenic and mutagenic (the content of, for example, chromium compounds). In addition, because its main feature, namely intense color, which is usually present even at low concentrations of dyes, wastewater containing dyes introduced into the aquatic environment without removing that type of contaminants will have a significant negative impact on the photosynthesis process due to significantly reduced light transmission through water [1].

A wide range of physical, chemical, and, in some cases, biological methods are used in the treatment of colored wastewater. The physico-chemical methods include the coagulation/flocculation process [2–8], chemical oxidation [9], advanced oxidation processes – AOPs [10–19], photodegradation [20–31], adsorption (using both conventional commercial adsorbents and adsorbents made from wastes so-called waste-sorbents or waste-based-sorbents [32–40]) and membrane filtration technics (nanofiltration and reverse osmosis [41–45]) are used.

This publication describes the results of the adsorption process of two different dyes on the surface of the adsorbent produced from water treatment residuals named post-coagulation sludge. The cationic dye Methylene blue and the anionic dye Direct red 81 were used in the studies. As part of the research, a series of experiments were conducted to determine the effect of the conditions of the adsorption process on its effectiveness, as well as to determine the adsorption kinetics and adsorption isotherms.

Methylene blue belongs to the thiazine dye group. Excessive amounts of this dye can have a negative impact on the aquatic environment, animals, plants, and people. In the case of the aquatic environment, the excess of this dye inhibits the photosynthesis process, which reduces the degree of water oxygenation and may result in the eutrophication of aquatic ecosystems. In the case of plants, excess Methylene blue (MB) can inhibit their growth, and reduce the amount of pigment and content in microalgae. About humans, the negative impact on the human body can be manifested by such symptoms as dizziness, headache, upset stomach and stomach cramps, nausea, vomiting, cyanosis, tissue necrosis, jaundice, and accelerated heartbeat [46–48].

Direct red 81 belongs to the group of sulfonated azo-based dyes. These dyes are toxic, carcinogenic, and mutagenic to humans and animals. Therefore, they can also lead to mutations in aquatic organisms. In addition, these dyes can lead to the formation of cancer and various types of allergies. About humans, the negative impact of this dye on human health may also be manifested by the occurrence of nausea, haemorrhage, ulceration of the skin and mucous membranes, anaemia, dermatitis, and kidney disease [49–51].

The sludge formed in water treatment processes using the coagulation/flocculation method was applied as an adsorbent in the experiments. So far, this sludge has only been dewatered and disposed of. Thanks to the proposed solution of using these sludges as the adsorbent, this waste is given a new, second life, which is in line with the assumptions of the circular economy [52].

In the case of MB, for its removal, adsorbents made from different materials have been applied. Examples of such adsorbents are as follows: organo-modified clay [53], hybrid sorbents synthesized from technical lignin's and silica [54], biochar from lychee seed [55], or iron modified *Pyrus pyrifolia* peels biochar [56]. For Direct red 81 (DR 81) adsorption, the following materials, among the others, were used: neutral soil containing copper [57], native bamboo sawdust [58], and citric acid modified bamboo sawdust [58]. However, in previous studies, sludge generated in water purification processes was not used.

In addition, the research proposed an innovative approach to the use of impedance measurement as one of the ways to characterize the surface and material of the adsorbent before and after the adsorption process.

Using impedance spectroscopy methods, it is possible to analyze the condition of the material by the relationships between it and measurable electrical and magnetic quantities. The parameter describing the material is the dynamic magnetic permeability. Changes in dynamic magnetic permeability can be studied indirectly when observing changes in the impedance of the coil in which the tested material is placed. The effective magnetic permeability is presented as a complex quantity, characterizing the state of the material in an alternating magnetic field, depending on the diameter of the sample, the specific conductivity γ, magnetic permeability of material of the sample μ_r, and the frequency of the voltage excitation signal f. An empty test coil with resistance Ro when connected to an AC voltage source has impedance Z_o. Inserting the test material into the coil, which acts as a core, causes the impedance to increase to the value of Z. The R_0 component of the Z impedance increases to the value of R.

2. Materials and methods

2.1. Characteristics of the adsorbates (dyes)

2.1.1. Methylene blue

Methylene blue (in this article referred to as MB) is a dye called Basic blue 9 with C.I. number 52015. When dissolved in water, it gives a deep dark blue color. It is a cationic dye belonging to the thiazine group. Its molecular weight is 319.85 g/mol, and its molecular formula is $C_{16}H_{18}N_3ClS$. This dye is widely used in biochemical applications as well as being used to treat anaemia and malaria, among others. It is also used for coloring wool, cotton, paper, and silk [59].

2.1.2. Direct red 81

Direct red 81 (in this article referred to as DR 81) belongs to the group of anionic azo dyes. It has two azo bonds in its chemical structure. It is a compound with a molecular weight of 975.6 g/mol and molecular formula $C_{29}H_{19}N_5Na_2O_8S_2$. Its C.I. number is 28160. This dye has an intense dark red color in water solutions. It is widely used for coloring cotton, and viscose and also for paper color [60].

2.2. Methodology of adsorbent preparation

The residuals (also called post-coagulation sludge) formed during surface water treatment by volumetric coagulation/flocculation were used in the experiments. In this process, aluminum sulfate was used as a reagent. This sludge was characterized by high hydration 99.8% and the content of organic and mineral parts at the level of 51% and 49%, respectively.

The first step in the preparation of the adsorbent was the dehydration of the collected residuals to a dry matter concentration of 25% using a filter press. Then, the sludge was dried in a laboratory drier at 105°C and crushed into grains <0.25 mm in diameter. The sludge prepared in this way was used as an adsorbent in the batch adsorption process of two synthetic dyes: Direct red 81 and Methylene blue.

2.3. Characterization of adsorbent

To demonstrate the surface structure of this adsorbent, two types of microscopic images were taken (using a Delta Optical Genetic PRO biological microscope at 100 times magnification and scanning electron microscopy by using an electron microscope the Phenom ProX – SEM). In the case of using the biological microscope Delta Optical Genetic PRO, samples of the adsorbent in the form of powder were placed on a microscope slide and directly subjected to observations. In the case of the electron microscope, the procedure of analysis was the following: the prepared powder was applied to a carbon tape glued to the microscope stage. Then the stage was placed in the holder of the electron microscope. The morphology and elemental composition of the samples were examined by scanning electron microscopy (SEM). Moreover, the Fourier-transform infrared spectroscopy (FTIR) measurement was conducted (using the Thermo Scientific™ FTIR Nicolet™ iS50 spectrometer) to determine the functional groups present on the surface of the adsorbent, and the specific surface area was measured using the N_2 adsorption at 77 K method (Gemini VI of Micromeritics USA). The methodology of the specific surface area measurement and the FTIR measurement is the same as it was described in the paper by Pieczykolan and Krzyżowska [38]. In the case of FTIR measurement, the study with the Fourier-transform infrared spectroscope was carried out in the attenuated total reflection mode. It allows recording of the transmittance spectrum as a function of the wavenumber in the range from 400 to 3,500 cm^{-1}. In the case of specific surface area measurement before the measurement, the adsorbent was dried at 105°C in the helium flow for 5 h and then in the measuring station in vacuum to the final pressure of 0.001 torr at room temperature for 2 h. The adsorbent prepared according to this procedure was subjected to the N_2 adsorption at 77 K method using Gemini VI of Micromeritics from the USA.

In addition, the impedance for the adsorbent was measured before and after the adsorption process using the impedance spectroscopy method.

2.3.1. Methodology of impedance spectroscopy

The analytical consideration proposed by Förster and the applications described in the paper [61] introduced the concept of effective permeability μ_{sk} and the assumption that the real component R_0 for an empty test coil is ignored. Only the imaginary component ωL_0 and the real component R remain:

$$\frac{Z}{\omega L_o} = j\left(1-\eta+\eta\mu_r\mu_{sk}\right) \tag{1}$$

The normalized impedance components are described by Förster's [61] formulas [Eqs. (2) and (3)]:

$$\frac{\mathrm{Re}\,\underline{E}}{\underline{E_0}} = \frac{R-R_0}{\omega L_0} = \eta\mu_r\left(-\mathrm{Im}\underline{\mu_{sk}}\right) \tag{2}$$

$$\frac{\mathrm{Im}\,\underline{E}}{\underline{E_0}} = \frac{\omega L}{\omega L_0} = 1-\eta+\eta\mu_r\left(\mathrm{Re}\underline{\mu_{sk}}\right) \tag{3}$$

where η – coil fill factor, E and E_0 – induced voltages in the coil with the core and the empty coil, μ_r – relative magnetic permeability of the core, μ_{sk} – effective magnetic permeability depending, among other things, on the specific conductivity γ.

The coil fill factor is defined as the quotient of the sample diameter D_p to the diameter of the circular coil D_s.

$$\eta = \left(\frac{D_p}{D_{s\Phi}}\right)^2 \tag{4}$$

Förster proposed that the normalized impedance components be determined for each frequency f across the test range $\frac{\Delta R}{\omega L_0}, \frac{\omega L}{\omega L_0}$.

These three parameters in a three-dimensional space form characteristics depict the state of the material's physical parameters at a given moment in time.

The change in material properties is observed by comparing the characteristics of the adsorbent before adsorption with the adsorbent after adsorption of the dye at a given measurement frequency interval.

The examined adsorbent in the form of powder was placed inside the measuring coil in a suitable cuvette. The measuring coil was connected to an Agilent 4294A precision impedance analyzer. Tests were carried out in the frequency range of the signal applied to the sample from 40 Hz to 200 kHz and results were recorded for adsorbent before adsorption and adsorbent after MB adsorption, adsorbent after DR 81 adsorption samples.

2.4. Methodology of batch adsorption experiments

The experiments were conducted in three stages. At first, the determination of pH value on process efficiency was examined. The next step was to determine the effect of contact time on the adsorption efficiency. At this stage, the adsorption kinetics was also analyzed. The last, and third stage of the research were experiments related to the determination of the adsorption isotherm. Based on the results of this stage, the fit of five models of adsorption isotherms to the experimental results was analyzed. All dye adsorption experiments were conducted three times, using the same process conditions. The obtained concentration values are the arithmetic mean of the results obtained in triplicate.

The efficiency of the adsorption process was assessed based on the value of the amount of the dye adsorbed per unit of adsorbent q_e [Eq. (5)] and based on the effectiveness of dye removal from the aqueous solution ξ [Eq. (6)].

$$q_e = \frac{\left(C_0 - C_e\right)}{m_{sl}} \tag{5}$$

$$\xi = \frac{\left(C_0 - C_e\right)}{C_0} \tag{6}$$

where q_e – the amount of dye adsorbed (mg/g), C_e – the dye concentration at equilibrium (mg/dm^3), C_0 – the initial dye concentration (mg/dm^3), m_{sl} – the amount of adsorbent (g/dm^3).

2.5. Effect of pH value

The first stage of the studies was connected with the determination of the influence of the pH of the dye solution on the effectiveness of the adsorption process. At this stage, the most favorable pH value was determined, at which the highest efficiency of dye adsorption was obtained.

For this purpose, a series of experiments were carried out in which five different pH values: 2, 4, 6, 8, and 10 were used, while constant values of the initial concentration of the dyes (C_0 = 50 mg/dm^3), the constant amount of adsorbent (2 g/dm^3) and a constant contact time (t = 60 min) were applied. The dye solution of 50 cm^3 with a specific pH value was introduced into 250 cm^3 conical flasks (the required pH value was adjusted with either 50% H_2SO_4 or 5% NaOH). The adsorbent was added to these solutions, the flasks were placed on a laboratory shaker (GFL 3005) and shaken for 60 min. After this time, the adsorbent was separated from the dye solutions by centrifugation, and the final concentrations of the dyes were measured. The concentration of the dyes was determined using the colorimetric method by measuring the absorbance of the solutions using the WTW SpectroFlex 6100 spectrophotometer (based on the previously prepared standard curves and at appropriate wavelengths – for DR 81 dye λ = 498 nm, for MB dye λ = 582 nm).

2.6. Effect of contact time

To determine the effect of the contact time on adsorption effectiveness a series of experiments were conducted for two different initial concentrations of the dyes (100 and 500 mg/dm^3) and for different contact times in the range of 5–180 min. In those experiments, a constant pH value of adsorption (determined based on the results of the first stage of the studies) and a constant amount of adsorbent (2 g/dm^3) were used. The methodology of conducting the process was the same as in the case of determining the influence of the pH value on the effectiveness of the process.

2.7. Kinetics studies

To examine the type of adsorption process, the results obtained in the second stage of the studies (connected with determining the impact of contact time on the effectiveness of the process) were analyzed in terms of determining the adsorption kinetics. Three models of kinetics were analyzed: pseudo-first-order [Eq. (7)] [62], pseudo-second-order [Eq. (8)] [63], and Elovich [Eq. (9)] [64,65]. The values of parameters of those kinetics models were estimated using non-linear regression by minimizing the error value RMSE [Eq. (11)] using Microsoft Office 365 Solver add-in.

In addition, the intraparticle diffusion model [Eq. (10)] was analyzed to understand the adsorption mechanism [66,67]. The parameters of this model were determined by linear estimation by preparing plot q_t vs. $t^{0.5}$ [68].

$$q_t = q_e \cdot \left(1 - \exp\left(-k_1 \cdot t\right)\right) \tag{7}$$

$$q_t = \frac{q_e^2 \cdot k_2 \cdot t}{1 + q_e \cdot k_2 \cdot t} \tag{8}$$

$$q_t = \frac{1}{b} \cdot \ln\left(1 + a \cdot b \cdot t\right) \tag{9}$$

$$q_t = K_{IPD} \cdot t^{0.5} + C \tag{10}$$

$$\mathrm{RMSE} = \sqrt{\frac{1}{n-2}\sum_{i=1}^{n}\left(q_{e,\exp} - q_{e,\mathrm{calc}}\right)_i^2} \tag{11}$$

where q_t – the amount of dye adsorbed after each contact time (mg/g), q_e – the amount of the adsorbed dye at equilibrium state (mg/g), k_1 – the constant rate of the pseudo-first-order model (1/min), k_2 – the constant rate of the pseudo-second-order model (g/(mg·min)), a – regarded as the initial sorption rate (mg/(g·min)), b – constant related to the extent of surface coverage, t – contact time (min), $q_{e,\exp}$ – the amount of dye adsorbed during the experiments (mg/g), $q_{e,\mathrm{calc}}$ – the estimated value of the amount of dye adsorbed (mg/g), K_{IPD} – the intraparticle diffusion rate constant (mg/(g·min$^{0.5}$)), C – a constant depicting the boundary-layer effects (mg/g).

2.8. Adsorption isotherm studies

In the third stage of studies, the experiments were carried out to determine the adsorption isotherm. In this case, for the constant contact time of the adsorbent with the dye, the constant values of pH, and the constant amount of adsorbent, different values of the initial concentration of dyes in the range of 50–2,000 mg/dm^3 were used. The values of pH and contact time were determined as a result of the first and second stages of studies. All adsorption isotherm studies were conducted at one temperature equalled 20°C.

All of the isotherm' models, their formulas, and parameter definitions are included in Table 1.

The results of this stage of experiments were applied to analyze the fit of five models of adsorption isotherms and to choose the model that best describes the experimental data. For this purpose, a non-linear regression method based on minimizing the error RMSE [Eq. (11)] was used. Moreover, the degree of fit of each isotherm model to the experimental data was determined based on the calculated correlation coefficient R^2.

In addition, the maximum adsorption capacity, adsorption energy, degree of heterogeneity of the system, and the type of adsorption process were estimated, through analysis of the values of determined parameters of adsorption isotherms.

Table 1
Isotherm' models

Isotherm model	Non-linear formula	References
Freundlich	$q_e = K_F \cdot C_e^{1/n}$	[69]
Langmuir	$q_e = \frac{q_m \cdot K_L \cdot C_e}{1 + K_L \cdot C_e}$	[70]
Jovanovic	$q_e = q_{\max} \cdot \left[1 - \exp\left(-K_J \cdot C_e\right)\right]$	[71]
Dubinin–Radushkevich	$q_e = Q_s \cdot \exp\left(-K_{\mathrm{DR}} \cdot \varepsilon^2\right)$ $\varepsilon = \mathrm{RT} \cdot \ln\left(1 + \frac{1}{C_e}\right)$ $E = \frac{1}{\sqrt{2 \cdot K_{\mathrm{DR}}}}$	[72]
Sips	$q_e = \frac{q_{\mathrm{mS}} \cdot K_S \cdot C_e^{\mathrm{SP}}}{1 + K_S \cdot C_e^{\mathrm{SP}}}$	[73]

q_e – the amount of dye adsorbed per gram of the adsorbent at equilibrium (mg/g); C_e – the equilibrium dye concentration (mg/dm^3); K_L – Langmuir isotherm constant (dm^3/mg); q_m – maximum monolayer capacity in Langmuir model (mg/g); n – Freundlich isotherm constant related to the heterogeneity of the process (–); K_F – Freundlich isotherm constant connected with relative adsorption capacity [(mg/g)(L/mg)$^{1/n}$]; Q_s – theoretical isotherm saturation capacity in Dubinin–Radushkevich model (mg/g); K_{DR} – the Dubinin–Radushkevich model constant related to the adsorption energy (mol^2/kJ^2); E – average free energy adsorption (kJ/mol); ε – Polanyi adsorption potential; R – universal gas constant; T – temperature (K); K_J – Jovanovic isotherm constant related with adsorption energy (dm^3/g); $q_{\max}$ – maximum adsorption capacity in the Jovanovic model (mg/g); q_{mS} – maximum monolayer adsorption capacity in Sips model (mg/g); K_S – constant related with energy of sorption and affinity of the system (dm^3/mg); SP – constant which represents the heterogeneity of the process (–).

3. Results and discussion

3.1. Characteristic of the adsorbent

3.1.1. Textural characterization

The general image of the adsorbent, when a hundred times magnification was used, is shown in Figs. 1–3. The adsorbent before the adsorption process is shown in Fig. 1. It can be seen that it is light brown in color and its surface is relatively highly differentiated. The next two figures show the adsorbent after the adsorption process of the two tested dyes: MB (Fig. 2) and DR 81 (Fig. 3). A significant change in the color of the used adsorbent is visible – after the process, it took on the color of the removed dye. In the case of MB adsorption, the adsorbent has an intense blue color after the process, and for DR 81 – intense red. This confirms that the process of adsorption or stopping of dye molecules on the surface of the tested adsorbent took place in the conducted experiments.

Fig. 1. Microscopic image of adsorbent before the adsorption process.

Fig. 4 shows the surface structure of the adsorbent by using SEM when two different image magnifications are applied. In Fig. 4a, the image shows the adsorbent at 1,250 times magnification, and in Fig. 4b – at 10,000 times magnification. Analyzing the obtained SEM images, it can be observed that the adsorbent has a relatively slightly corrugated surface. It can also be seen that the porosity of this material is not very high. The surfaces of the adsorbent grains are relatively flat with small depressions. However, the measured Brunauer–Emmett–Teller (BET)-specific surface area was 142.8651 m^2/g. Therefore, the specific surface area of the tested adsorbent is relatively small but comparable to adsorbents obtained from such waste materials as, for example, non-activated carbonized sewage sludge (non-activated carbonized sewage sludge 202 m^2/g [74]), biochar derived from mango leaves (168.23 m^2/g [37]). The value of BET of tested adsorbent is relatively slightly smaller than the surface of adsorbents obtained from activated

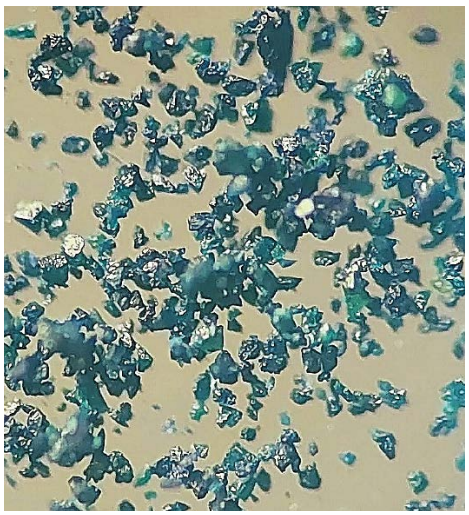

Fig. 2. Microscopic image of adsorbent after Methylene blue adsorption.

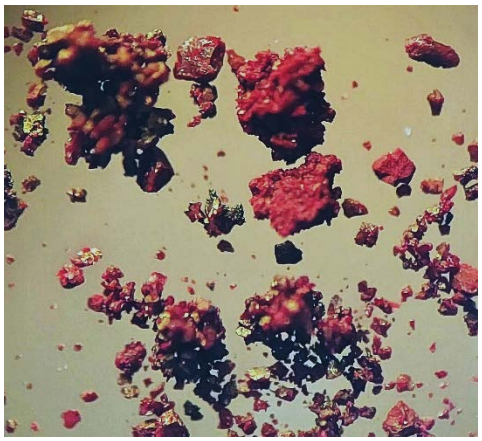

Fig. 3. Microscopic image of adsorbent after Direct red 81 adsorption.

sludge subjected to various processes of carbonization and chemical or physical activation (surplus biological sludge – 253 m^2/g [75]) or adsorbents generated from textile sewage sludge (310–336 m^2/g [76]).

3.1.2. FTIR measurements

The results of the FTIR measurement for the adsorbent are shown in Fig. 5. By analyzing the graph of the dependence of the transmittance on the wavenumber, the presence of the following functional groups on the adsorbent surface was found: groups with C≡C or C≡N bonds; O–H and C=N bonded groups; C–O or C–O–C groups. A detailed analysis of the FTIR measurement results made for this sorbent is described in the publication by Pieczykolan and Krzyżowska [38].

3.1.3. Impedance spectroscopy

The frequency characteristics of inductance L_S and resistance R_S in series, as well as impedance modulus Z and phase shift angle θ were recorded.

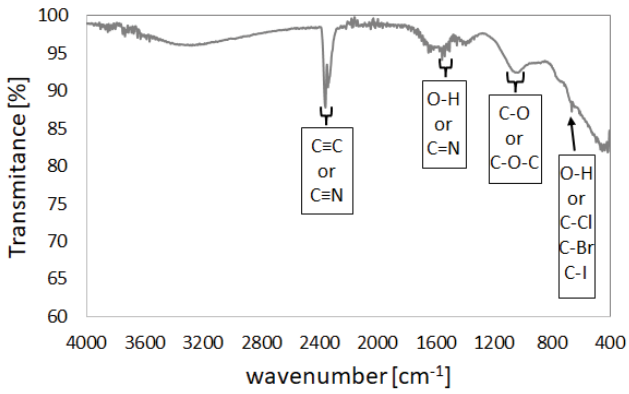

Fig. 5. Fourier-transform infrared spectroscopy measurement.

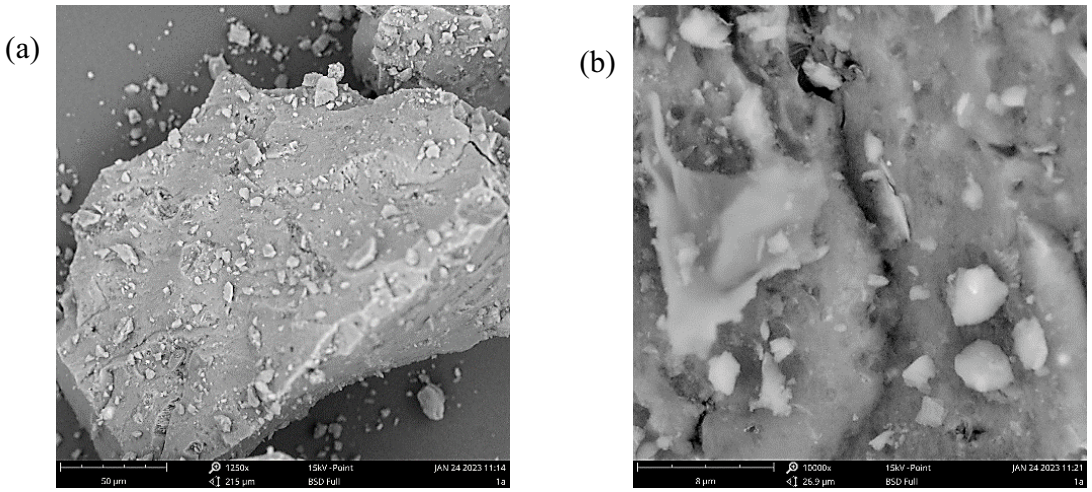

Fig. 4. SEM images of adsorbent before the adsorption process with a magnification of: (a) 1,250 times and (b) 10,000 times.

The changes due to the differences between the adsorbent before adsorption process and adsorbent after MB and DR 81 adsorption are analyzed (Fig. 6).

According to Eqs. (2) and (3), and after taking into account the filling factor η [Eq. (4)], the changes in the real and imaginary part of the normalized components of impedance were determined, which made it possible to determine the dynamic values of the effective magnetic permeability and specific conductivity of the material (Fig. 6).

The measurement frequency interval from 123 to 135 kHz reveals significant changes in impedance components and changes in electrical and magnetic parameters. No changes of a similar nature were registered in the high measurement frequency intervals.

The analysis of the absolute changes in the impedance components shows that the influence of the dyes used in the process varies, as presented in Fig. 7.

Significant changes in the normalized real component of the impedance can be seen, which directly indicates the electrical conductivity. A decrease in the value of the real component indicates that the MB dye deteriorates the electrical properties, and the DR 81 dye improves them. Thus, the effect of the dye on the electrical properties of the adsorbent requires further electrical studies.

Changes in the normalized imaginary component of the impedance are negligibly small and indicate that there is no significant change in magnetic permeability.

3.2. Effect of pH

The conducted experiments showed a very significant influence on the efficiency of the pH value at which the adsorption process was carried out. Two dyes of different characteristics were used in the tests: anionic DR 81 and cationic MB. This difference had a very large impact on the most favorable pH value, at which the highest efficiency of each dye removal was achieved.

During the adsorption of DR 81 onto the adsorbent, a very substantial influence of the pH value on the removal efficiency was noted (Fig. 8a). It was observed that only the use of a very low pH value contributed to adsorbing the DR 81 dye on the surface of the adsorbent. At pH 2, the highest degree of DR 81 removal ξ was obtained, amounting up to 99.8%, and the concentration of the dye decreased from the initial value of 50 up to 0.12 mg/dm^3. Using pH values higher than 2, the efficiency of the process ξ decreased to approx. 77.0% (DR 81 concentration after the adsorption process was in the range of 11.3–11.7 mg/dm^3).

In the case of MB, the pH value also had an important impact on dye removal. However, no such huge differences

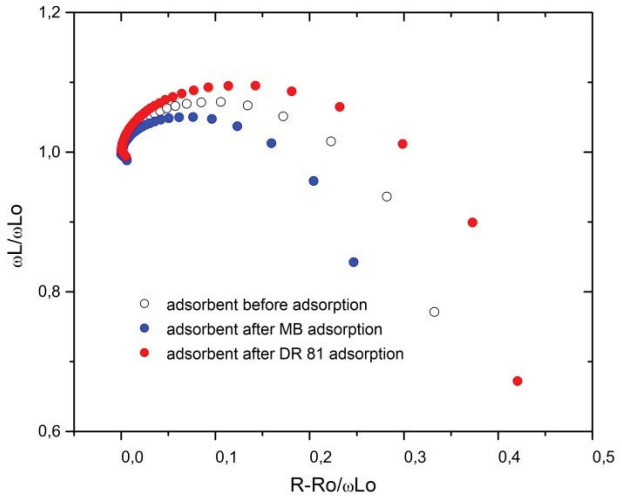

Fig. 6. Characteristics describing the direction of changes in the impedance component values in relation to the base material.

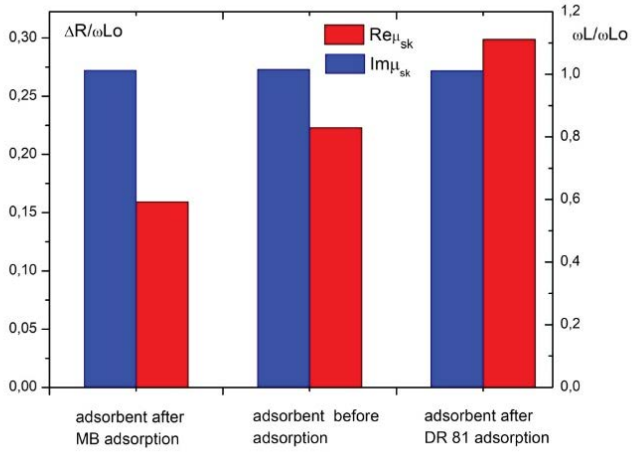

Fig. 7. Changes in the normalized impedance components for one of the points of the maximum detection sensitivity area.

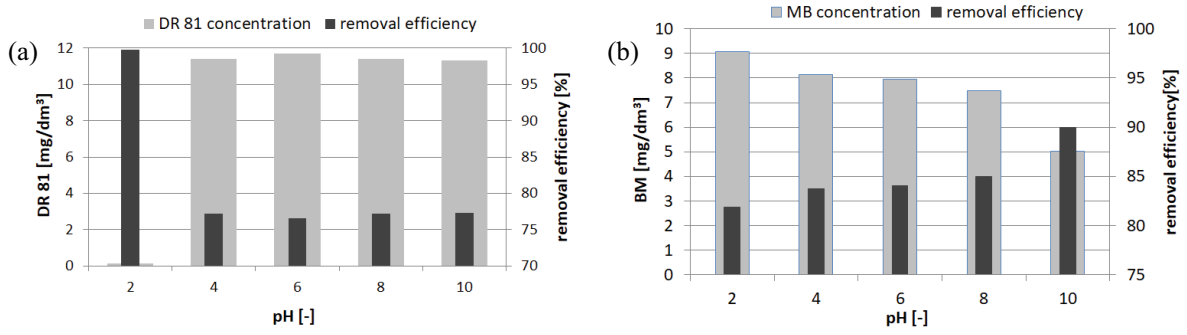

Fig. 8. Effect of pH value on dye concentration and efficiency of the process for: (a) Direct red 81 and (b) Methylene blue.

in effectiveness were noted when different pH values were used. The greatest degree of dye removal was ξ = 90.0% and it was obtained when the pH value equalled 10 (Fig. 8b). The dye concentration after the process was 5 mg/dm^3. Using smaller pH values, a lower efficiency of the process was observed – as the pH value decreased from 8 to 2, the value of dye removal ξ gradually decreased from 85.0% to 81.9%.

The observed differences in changes in effectiveness with a change in pH value may indicate that the surface charge of the tested adsorbent was negative. Therefore, in the case of the cationic MB dye, increasing the pH did not result in such a significant increase in effectiveness as in the case of the DR 81 anionic dye. In this case, only the use of a strongly acidic adsorption environment resulted in the adsorption process – it was caused by the phenomenon of surface protonation, which caused the surface charge of the adsorbent to assume a positive value.

The conducted tests also showed that when using the most favorable pH value for each dye (for DR 81 pH = 2.0, and for MB pH = 10.0), a higher value of adsorbed dye was obtained for DR 81 (q_e = 24.9 mg/g) than for MB (q_e = 22.5 mg/g). However, in the case of DR 81, the use of a pH above 2 resulted in a decrease of the adsorbed amount of dye to approx. 19.3 mg/g regardless of the pH used (Fig. 9a). In contrast, during the adsorption of MB, the difference in the amount of adsorbed dye was not so significant and decreased from 22.5 mg/g for pH 10 to the level in the range of 20.5–21.3 mg/g for pH in the range 2–8 (Fig. 9b).

3.3. Effect of contact time

Experiments connected with determining the impact of contact time on the effectiveness of the adsorption process were carried out for the following process parameters:

- for MB: pH = 10, C_0 = 100 and 500 mg/dm^3, amount of adsorbent = 2 g/dm^3,
- for DR 81: pH = 2, C_0 = 100 and 500 mg/dm^3, amount of adsorbent = 2 g/dm^3.

The conducted studies showed that for both dyes, the adsorption process proceeds the fastest in the first minutes (Figs. 10 and 11).

In the case of the MB, after the first 5 min of contact time, the final concentration of the dye was significantly decreased for both initial concentrations (Fig. 10b). Extending the contact time didn't significantly contribute to the decrease in the value of the concentration. In addition, in the case of MB, it can be observed that the dye removal efficiency ξ was similar for both initial concentrations, when the contact time was longer than 5 min – it was at the level of 84%–89% and 78%–81% for the initial concentration of 100 and 500 mg/dm^3, respectively (Fig. 10a).

In the case of the DR 81, also after the first 5 min of contact time, the greatest decrease in concentration in the solution was observed (Fig. 11b). In this case, however, extending the time resulted in a further decrease in the concentration of DR 81, but these changes were much smaller in comparison

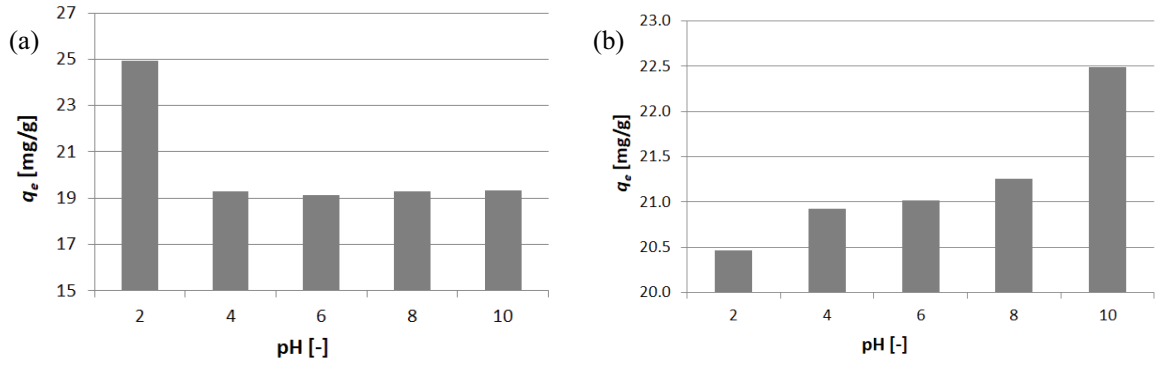

Fig. 9. Effect of pH value on the amount of dye adsorbed for: (a) Direct red 81 and (b) Methylene blue.

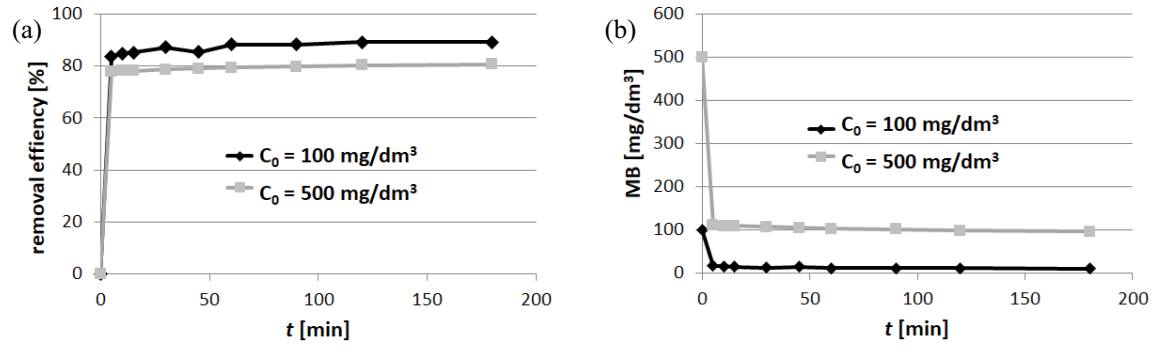

Fig. 10. Effect of contact time for Methylene blue: (a) removal efficiency and (b) final dye concentration.

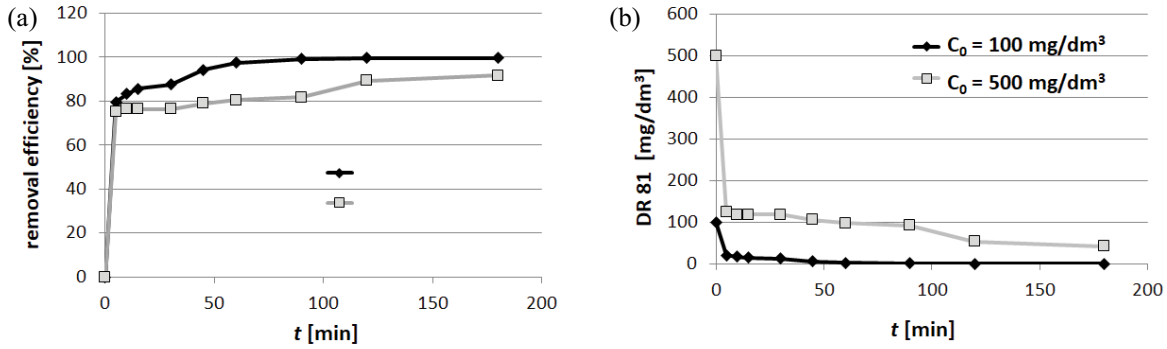

Fig. 11. Effect of contact time for Direct red 81: (a) removal efficiency and (b) final dye concentration.

with the initial 5 min. Moreover, more significant differences in the degree of dye removal were observed depending on the initial concentration (Fig. 11a). For the concentration of 100 mg/dm^3, almost complete removal of the dye was obtained after 60 min of contact, while for the concentration of 500 mg/dm^3, the time needed to obtain the highest degree of removal was 120 min. Therefore, based on the obtained test results, 30 min was established as the most favorable contact time for MB and 90 min for DR 81.

Analyzing the obtained results of the impact of contact time on the process efficiency, it can also be observed that a very high removal efficiency was obtained for both dyes, with a slightly higher degree of removal for DR 81.

The results of the impact of contact time on the effectiveness of dye removal obtained in the conducted research correspond to the results of other researchers. A similar effectiveness of MB and DR 81 removal depending on the contact time was reported in studies using calcined magnesite as an adsorbent [65]. Also in this case, for MB, the stabilization of the dye removal degree at a quite similar level took place earlier than for DR 81. For DR 81, bamboo adsorbent and treated bamboo sawdust were used for the adsorption of this dye [58]. The results of those tests indicated that a period of about 70–80 min was still necessary for the degree of dye removal to stabilize. In contrast, the conducted MB adsorption studies on the adsorbent derived from *Argania spinosa* showed, similarly to the studies described in this publication, that a relatively short contact time of 30 min was required to achieve stable values of the degree of removal, regardless of increasing the contact time [77]. However, in the case of studies conducted by Pieczykolan and Krzyżowska [38] with the use of dried water treatment residuals for the adsorption of the Reactive blue 81, a time of 90 min was necessary to achieve a stable efficiency of removing this dye.

3.4. Kinetic studies

The results of the experiments carried out in the second stage were used to determine the parameters of three models of adsorption kinetics. Based on the estimation results, it was also determined which of the analyzed kinetics models describes the best experimental data results (based on the determined value of the correlation coefficient R^2).

The results showed that for both dyes, the model of adsorption kinetics, for which the highest degree of adjustment to the experimental results was obtained, is the Elovich model. In the case of DR 81, R^2 was 0.949 and 0.741 for the initial dye concentration of 100 and 500 mg/dm^3, respectively (Table 2). For the MB, the values of R^2 were 0.963 and 0.938 for the initial dye concentration of 100 and 500 mg/dm^3, respectively. In the case of pseudo-second-order kinetics, a relatively high degree of fit of this model to the results obtained in the tests was obtained for the initial concentrations of dyes equal to 100 mg/dm^3 (for both dyes). However, when higher concentrations were used, the degree of fit of this model expressed by the value of R^2 decreased significantly.

The studies showed that with the increase in the initial concentration of both dyes, the constant-rate in the pseudo-second-order kinetics model decreased (Table 2). This phenomenon may result from the greater competition faced by dye molecules for unoccupied active sites at higher concentrations, causing less dye adsorption, hence low k_2 values [78].

While analyzing the determined values of the amount of the adsorbed dye at equilibrium state q_e, it can be seen that the values were more similar to the experimental data for the pseudo-second-order model than for the pseudo-first-order model. For example, for the MB at the initial concentration of 100 mg/dm^3, the estimated q_e was 43.8 and 44.3 mg/g for the pseudo-first-order and pseudo-second-order models, respectively, while the q_e value obtained as a result of the experiments was 44.6 mg/g.

Estimated values of adsorption rate constants in the Elovich model (as well as from pseudo-second-order) indicate that higher values were obtained for the adsorption process of the MB than for the DR 81. In addition, in the case of MB, the use of a higher initial concentration resulted in a very significant increase in the adsorption rate, which may be related to the expected surface electrical charge of the tested adsorbent (studies of the effect of pH on the adsorption efficiency indicated that the surface charge of the adsorbent may be negative). Thus, the obtained results of the analysis of the three selected kinetics models indicate that chemical adsorption for both dyes occurred. Both the pseudo-second-order model and the Elovich model are used to describe the kinetics of the chemical adsorption process [79–83]. Elovich kinetic model is used to describe the rate of adsorption that decreases exponentially with an increase in the amount of adsorbate [83,84].

Table 2
Parameters of adsorption kinetics

Kinetics model	Initial dye concentration	Parameter	Unit	Dye	
				Direct red 81	Methylene blue
Pseudo-first-order	100 mg/dm³	k_1	1/min	0.3265	0.6120
		q_e	mg/g	47.1	43.8
		R^2		0.459	0.428
	500 mg/dm³	k_1	1/min	0.4810	0.6120
		q_e	mg/g	203.9	198.9
		R^2		0.140	0.234
Pseudo-second-order	100 mg/dm³	k_2	g/(mg·min)	0.0136	0.0639
		q_e	mg/g	49.1	44.3
		R^2		0.811	0.855
	500 mg/dm³	k_2	g/(mg·min)	0.0056	0.0312
		q_e	mg/g	210.0	199.5
		R^2		0.400	0.605
Elovich	100 mg/dm³	a	mg/(g·min)	1.587105	2.441021
		b	g/mg	0.314	1.218
		R^2		0.949	0.963
	500 mg/dm³	a	mg/(g·min)	4.053107	4.591040
		b	g/mg	0.093	0.488
		R^2		0.741	0.938

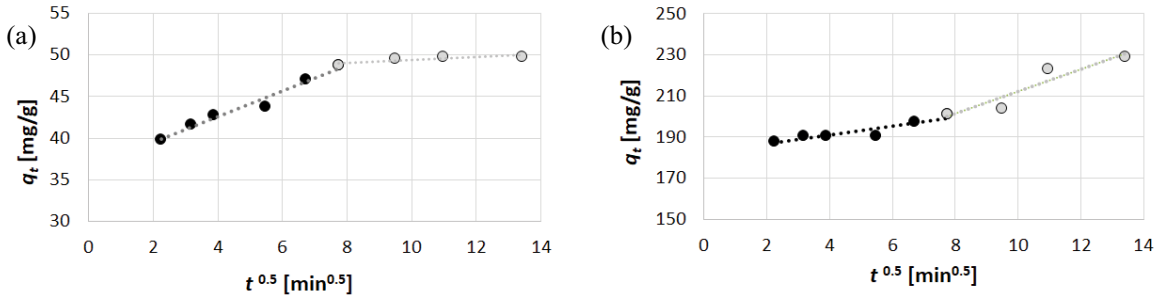

Fig. 12. Intraparticle diffusion plot for Direct red 81: (a) 100 mg/dm³ and (b) 500 mg/dm³.

The results of the analysis of models of adsorption kinetics obtained in these experiments are similar to the results obtained in adsorption processes using other types of adsorbents. Concerning MB, in the case of adsorption of this dye onto acid washed black cumin seed powder material [85], adsorption onto modified activated carbon by carboxylic group (–COOH) via AC mechanical attrition [86], adsorption onto multiwalled carbon nanotubes functionalized with L-tyrosine [79] as well as adsorption on hollow silica nanoparticles [87] also obtained the best fit of the pseudo-second-order kinetics model, as was achieved in the studies described in this article.

In the case of the DR 81, similar results to those obtained in this article, in which the pseudo-second-order kinetics model well described the experimental results, were obtained when *Argemone mexicana* seeds [50], or native and citric acid modified bamboo sawdust [58], or soy meal hull [88] were applied as adsorbents.

Based on analyzing the results of the intraparticle diffusion model, the adsorption mechanism for both tested dyes can be concluded. Plots of $q_t = f(t^{0.5})$ were made for both dyes and both initial concentrations (Figs. 12 and 13). For the lower initial concentration of 100 mg/dm³, a clear division into two stages was observed for both dyes, with the first stage being much sharper than the second. However, when higher values of the initial concentration were used for both dyes, the division into two stages on the graph is much less visible.

However, in general, two stages can be distinguished in the intraparticle diffusion model plots for both dyes. The first portion (sharpened portion) of the curve shows the film diffusion process, in which dye molecules move to the vicinity of the adsorbent surface from the depth of the solution. This process is also called outer diffusion [89–91]. The second stage, which is visible in the graphs, illustrates the process of inner diffusion, also called intraparticle diffusion.

In this stage of adsorption, dye molecules move from the external surface of the adsorbent into its pores [89,92]. In the case of an adsorption process, typically this second step is the rate-limiting one for the entire adsorption process. In the case of the conducted experiments, for the initial concentration of 100 mg/dm^3, the adsorption rate determined from the intraparticle diffusion model is much lower for the second stage – that is, for the inner diffusion process (Table 3). In the case of the DR 81 dye, the difference of the adsorption rate between the first and second stage was almost nine times. For the MB dye, that difference was slightly less significant – the K_{IPD} value decreased by approx. 5 times.

It was also noted that the duration of the first stage (outer diffusion) and the second stage (inner diffusion) for both dyes is very similar. In the case of MB for the initial concentration of 500 mg/dm^3 and the dye DR 81 and both examined initial concentrations, the duration of each stage was 60 min. Only for MB and the initial concentration of 100 mg/dm^3, the duration of the second stage was longer by 15 min than the duration of the first stage. This phenomenon proves that in the case of adsorption of the tested dyes, not only inner diffusion but also outer diffusion played an important role in the rate of adsorption.

In the intraparticle diffusion model, the C parameter defines the influence of the boundary layer on the adsorption process. The higher the value of this parameter, the more significant the influence of the boundary layer on the speed of the external mass transfer process – because the thickness of the boundary layer increases [93–95]. In the studies, the value of parameter C was always greater than zero, with much higher values obtained for experiments in which the initial concentrations of dyes were 500 mg/dm^3. The tests also showed that slightly lower C values were obtained for the DR 81 than for MB.

3.5. Adsorption isotherm studies

The results of adsorption isotherm experiments showed that the Jovanovic isotherm model is the model with the highest degree of matches to experimental data for both dyes – the value of R^2 was 0.992 and 0.989 for DR 81 and MB, respectively (Table 4). A slightly lower degree of fitting was obtained for the Langmuir and Sips isotherm models. The Jovanovic isotherm model is essentially the same as that considered by Langmuir and describes localized monolayer adsorption without lateral interactions. It does, however, assume a further assumption related to the likely mechanical contact between adsorbate and adsorbent [96,97].

When analyzing the value of the maximum monolayer capacity determined from the Jovanovic model (q_{max}), it was noted that similar values of this parameter were obtained for both dyes, with a slightly higher value obtained for DR 81 adsorption – q_{max} were 871.61 and 823.06 mg/g for DR 81 and MB, respectively. However, the value of maximum monolayer adsorption capacity q_{mS} determined from the Sips model also indicates that its value was higher for the DR 81 dye than for MB, however in this case the difference between these values is almost two times.

Also, the K_F parameter in the Freundlich model is a constant related to the relative adsorption capacity [98,99]. The K_F values obtained by estimation also indicate that a higher adsorption capacity was obtained for the DR 81 dye – the K_F value was equal to 10.504 [(mg/g)(L/mg)$^{1/n}$] and 7.707 [(mg/g)(L/mg)$^{1/n}$] for DR 81 and MB, respectively.

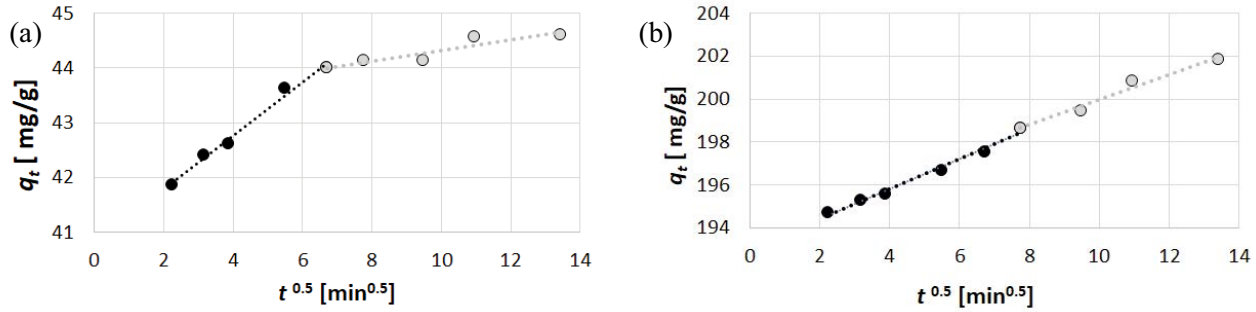

Fig. 13. Intraparticle diffusion plot for Methylene blue: (a) 100 mg/dm^3 and (b) 500 mg/dm^3.

Table 3
Parameters of the intraparticle diffusion model

Parameters	Type of dye							
	Direct red 81				Methylene blue			
	100 mg/dm^3		500 mg/dm^3		100 mg/dm^3		500 mg/dm^3	
	First stage	Second stage	First stage	Second stage	First stage	Second stage	First stage	Second stage
K_{IPD}	1.5451	0.1756	2.1491	5.4706	0.478	0.0982	0.6976	0.5901
C	36.427	47.643	182.57	157.45	40.819	43.349	193.02	194.08
R^2	0.972	0.667	0.845	0.886	0.988	0.853	0.988	0.973

The parameter 1/*n* in the Freundlich model indicates the heterogeneity of the system, the lower the value of this parameter, the greater the heterogeneity of the system [99,100]. Also, the value of the *SP* constant in the Sips isotherm model determines the degree of heterogeneity of the adsorbent surface – the closer the value of this parameter to 0, the greater the heterogeneity of the adsorbent surface [101,102]. In the case of the Sips model, high values of the *SP* parameter, very close to, or even equal to 1, were obtained for both dyes (Table 4). This indicates a small heterogeneity or even homogeneity of the surface of the adsorbent. Also, the values of the 1/*n* parameter in the Freundlich model for both dyes were high and relatively close to one.

Table 4
Values of isotherm parameters obtained during estimation

Isotherm model	Parameter	Type of dye	
		Direct red 81	Methylene blue
Freundlich	1/*n*	0.659	0.707
	K_F	10.504	7.708
	R^2	0.988	0.976
	RMSE	24.59	31.63
Langmuir	q_m	1,333.4	1,298.9
	K_L	0.0018	0.0018
	R^2	0.991	0.988
	RMSE	25.31	22.57
Jovanovic	q_{max}	871.6	823.1
	K_J	0.0026	0.0027
	R^2	0.992	0.989
	RMSE	25.38	20.75
Dubinin–Radushkevich	Q_s	361.6	58.6
	K_{DR}	0.39968	2700.71
	E	1.12	0.01
	R^2	0.156	0.946
	RMSE	203.02	61.01
Sips	q_{mS}	2,475.5	1,298.9
	K_S	0.0024	0.0018
	SP	0.8005	1
	R^2	0.990	0.988
	RMSE	23.47	22.57

In the Langmuir model the K_L parameter, in the Jovanovic model the K_J parameter, and in the Sips model the K_S parameter are constants related to the free adsorption energy. These parameters also indicate an affinity for the surface [96,98,103–105]. When analyzing the obtained estimation results, it was noted that in the case of the Jovanovic and Langmuir models, the K_L and K_J parameters have very similar values for both dyes (Table 4). This proves that the adsorption energy for both dyes is similar. However, in the case of the Sips model, the value of the K_S parameter was higher for DR 81 adsorption than for MB, but the difference in the value of this parameter was relatively small. Based on the obtained results, it can also be concluded that both dyes have a similar affinity to the surface of the adsorbent used in the tests.

Table 5 presents exemplary results of removing MB and DR 81 when various types of waste-adsorbents were used. In the case of the DR 81, the determined adsorption capacity of the adsorbent (described in this publication) is much higher than the values obtained in the tests listed in Table 5. This value is almost three times higher than the adsorption capacity obtained when using magnetic graphene oxide coated with branched polyethyleneimine nanocomposite as an adsorbent.

Also, in the case of the cationic dye (MB) used in the tests described in this publication, the adsorption capacity is much higher than the adsorption capacities listed in Table 5 obtained in the adsorption process using various waste adsorbents.

4. Conclusions

Batch adsorption experiments connected with the application of the water treatment residuals, named also post-coagulation sludge, as an adsorbent for MB and DR 81 removal were carried out. For both dyes, a significant influence of the pH value on the efficiency of the process was noted. In the case of MB, significant adsorption efficiency was obtained at neutral and alkaline pH (the highest

Table 5
Sorption capacity for Methylene blue and Direct red 81 obtained while using different kinds of adsorbents

Dye	Type of adsorbent	Adsorption capacity	References
Direct red 81	Natural adsorbent, *Argemone mexicana*	2.4–6.9 mol/g	[50]
Direct red 81	Magnetic graphene oxide coated with branched polyethyleneimine nanocomposite	284.3 mg/g	[106]
Direct red 81	Neutral soil containing copper	26.2 mg/g	[57]
Direct red 81	Native bamboo sawdust	6.43 mg/g	[58]
Direct red 81	Citric acid modified bamboo sawdust	13.83 mg/g	[58]
Methylene blue	Organo modified clay	399.74 micromole/g	[53]
Methylene blue	Hybrid sorbents synthesized from technical lignin's and silica	60 mg/g	[54]
Methylene blue	Biochar from lychee seed	124.5 mg/g	[55]
Methylene blue	Garlic straw (GS) prepared from agricultural waste	256.41	[107]
Methylene blue	Kaolin	29.85 mg/g	[108]

efficiency was obtained for pH 10), while for DR 81, only the use of strongly acidic process conditions allowed adsorbing this dye. The studies of the impact of the contact time on the adsorption efficiency showed that the required contact time for MB was three times shorter (30 min) than for DR 81 (90 min). The experimental kinetics data for both dyes were well represented by Elovich and pseudo-second-order kinetics. This suggests a chemical adsorption process. In addition, the adsorption rate constant was much higher for MB adsorption than DR 81 – such a relationship was obtained in all analyzed models of kinetics. The equilibrium isotherm data analysis showed that the Jovanovic model and the Sips model had the best fit for the experimental results. The maximum adsorption capacity determined based on the Jovanovic model was similar for both tested dyes and was 871.6 and 823.1 mg/g for DR 81 and MB, respectively. The obtained value of the K_J parameter indicating the degree of affinity of the substance to the adsorbent surface was also similar for both dyes. The analysis of the determined $1/n$ values in the Freundlich model, as well as the values of SP exponent in the Sips model, indicate that the tested adsorbent was characterized by a relatively small surface heterogeneity.

The conducted experiments showed that water treatment residuals can be successfully used as an adsorbent and can be an interesting alternative to expensive commercial adsorbents. However, further research will be needed to determine the reproducibility and stability of the efficiency of this process. These studies will be a continuation and development of the studies conducted so far.

The results of the studies of the use of waste material as an adsorbent, proposed and described in the article, are part of sustainable environmental processes. Environmental sustainability consists in applying solutions aimed at improving the quality of human life in such a way as to minimize and limit the negative impact on the earth's ecosystem at the same time. Concerning this assumption, the solution proposed in the described studies reduces the negative impact of human activity on the natural environment, as it would reduce the consumption of natural resources used to produce classically activated carbons used for wastewater treatment in the adsorption process.

Moreover, the effective use of waste materials as adsorbents in the adsorption processes has a twofold beneficial effect on the natural environment. The first benefit resulting from the use of waste as a "raw material" for the production of the adsorbent is the reduction of the consumption of high-quality and expensive raw materials needed for the production of commercial adsorbents appearing as classically activated carbons. On the other hand, the second benefit is the reuse of waste that has already been created, thus giving them a "new life" in the service of environmental protection.

Acknowledgment

This work was supported by the Ministry of Science and the Higher Education Republic of Poland within statutory funds, 2023.

We thank dr inż. Marcin Jesionek from the Institute of Physics of the Silesian University of Technology for his help in taking the photos SEM included in the article.

References

[1] M.T. Yagub, T.K. Sen, S. Afroze, H.M. Ang, Dye and its removal from aqueous solution by adsorption: a review, Adv. Colloid Interface Sci., 209 (2014) 172–184.
[2] A.Y. Zahrim, N. Hilal, Treatment of highly concentrated dye solution by coagulation/flocculation-sand filtration and nanofiltration, Water Resour. Ind., 3 (2013) 23–34.
[3] H. Li, S. Liu, J. Zhao, N. Feng, Removal of reactive dyes from wastewater assisted with kaolin clay by magnesium hydroxide coagulation process, Colloids Surf., A, 494 (2016) 222–227.
[4] P.J. Quinlan, A. Tanvir, K.C. Tam, Application of the central composite design to study the flocculation of an anionic azo dye using quaternized cellulose nanofibrils, Carbohydr. Polym., 133 (2015) 80–89.
[5] S.S. Moghaddam, M.R.A. Moghaddam, M. Arami, Coagulation/flocculation process for dye removal using sludge from water treatment plant: optimization through response surface methodology, J. Hazard. Mater., 175 (2010) 651–657.
[6] K.E. Lee, N. Morad, T.T. Teng, B.T. Poh, Factorial experimental design for reactive dye flocculation using inorganic-organic composite polymer, APCBEE Procedia, 1 (2012) 59–65.
[7] Y.Y. Lau, Y.S. Wong, T.T. Teng, N. Morad, M. Rafatullah, S.A. Ong, Coagulation–flocculation of azo dye Acid orange 7 with green refined laterite soil, Chem. Eng. J., 246 (2014) 383–390.
[8] B. Liu, H. Zheng, Y. Wang, X. Chen, C. Zhao, Y. An, X. Tang, A novel carboxyl-rich chitosan-based polymer and its application for clay flocculation and cationic dye removal, Sci. Total Environ., 640–641 (2018) 107–115.
[9] S. Khorramfar, N.M. Mahmoodi, M. Arami, H. Bahrami, Oxidation of dyes from colored wastewater using activated carbon/hydrogen peroxide, Desalination, 279 (2011) 183–189.
[10] G. Harichandran, S. Prasad, SonoFenton degradation of an azo dye, Direct red, Ultrason. Sonochem., 29 (2016) 178–185.
[11] R.F.N. Quadrado, A.R. Fajardo, Fast decolorization of azo methyl orange via heterogeneous Fenton and Fenton-like reactions using alginate-Fe^{2+}/Fe^{3+} films as catalysts, Carbohydr. Polym., 177 (2017) 443–450.
[12] X.X. Xiaoguo Shi, A. Tian, J. You, H. Yang, Y. Wang, Degradation of organic dyes by a new heterogeneous Fenton reagent - Fe_2GeS_4 nanoparticle, J. Hazard. Mater., 353 (2018) 182–189.
[13] B. Zhu, H. Cheng, Y. Qin, J. Ma, Y. Kong, S. Komarneni, Copper sulfide as an excellent co-catalyst with $K_2S_2O_8$ for dye decomposition in advanced oxidation process, Sep. Purif. Technol., 233 (2020) 116057, doi: 10.1016/j.seppur.2019.116057.
[14] H. Song, C. Chen, H. Zhang, J. Huang, Rapid decolorization of dyes in heterogeneous Fenton-like oxidation catalyzed by Fe-incorporated Ti-HMS molecular sieves, J. Environ. Chem. Eng., 4 (2016) 460–467.
[15] I. Płonka, B. Pieczykolan, K. Barbusiński, J. Kalka, M. Thomas, P.J. Piskorz, Investigation of the efficiency of the UV/H_2O_2 process on the removal of dye Acid Green 16 from aqueous solutions: process optimization and toxicity assessment, Fibres Text. East. Eur., 25 (2017) 103–107.
[16] B. Rahimi, N.R. Rahimi, A. Ebrahimi, Catalytic reduction of hazardous Acid orange 10 dye by $BiVO_4$/TiO_2 nanocrystalline heterojunction and influence of aeration, $FeSO_4$, H_2O_2 and $FeCl_3$ on removal efficiency: a novel and environmentally friendly process, Arabian J. Chem., 15 (2022) 104003, doi: 10.1016/j.arabjc.2022.104003.
[17] A. Lassoued, J.F. Li, Influence of iron content in Fe-based amorphous alloy catalysts on degradation of azo dyes by fenton-like process, J. Phys. Chem. Solids, 180 (2023) 111475, doi: 10.1016/j.jpcs.2023.111475.
[18] R. Wang, J. Cao, J. Song, J. Liu, Y. Zhang, Application of boron doped diamond for electro-Fenton and photoelectro-Fenton decolorization of azo dye from dye-containing wastewater: Acid Red 1, Int. J. Electrochem. Sci., 17 (2022) 220249, doi: 10.20964/2022.02.45.
[19] Z. Bencheqroun, N.E. Sahin, O.S.G.P. Soares, M.F.R. Pereira, H. Zaitan, M. Nawdali, E. Rombi, A.M. Fonseca, P. Parpot, I.C. Neves, Fe(III)-exchanged zeolites as efficient

electrocatalysts for Fenton-like oxidation of dyes in aqueous phase, J. Environ. Chem. Eng., 10 (2022) 1–13.
[20] W. Zhong, H. Qiang, J. Jiang, Y. Wu, Y. Padwal, S.W. Gosavi, R. Chauhan, H. Sakiyama, M. Afzal, A. Alarifi, Syntheses, characterization of Ni(II)/Zn(II) complexes derived from flexible tricarboxylate ligand and 2,2′-bipyridine and their methyl violet dye photodegradation applications, J. Mol. Struct., 1287 (2023) 135718, doi: 10.1016/j.molstruc.2023.135718.
[21] W.N. Du, S.T. Chen, Photo- and chemocatalytic oxidation of dyes in water, J. Environ. Manage., 206 (2018) 507–515.
[22] D. Wei, X. Yang, Y. Liu, H. Jin Seo, Boosting photodegradation of dye solutions based on Eu^{3+} doping in Bismuth-layered oxyhalogenide semiconductor $NaBi_3O_4Cl_{1.5}Br_{0.5}$, Appl. Surf. Sci., 567 (2021) 150814, doi: 10.1016/j.apsusc.2021.150814.
[23] S. Garg, N. Goel, Photodegradation of dye using polythiophene/ZnO nanocomposite: a computational approach, J. Mol. Graphics Modell., 117 (2022) 108285, doi: 10.1016/j.jmgm.2022.108285.
[24] R. Yuan, S.N. Ramjaun, Z. Wang, J. Liu, Photocatalytic degradation and chlorination of azo dye in saline wastewater: kinetics and AOX formation, Chem. Eng. J., 192 (2012) 171–178.
[25] A. Jamil, T.H. Bokhari, T. Javed, R. Mustafa, M. Sajid, S. Noreen, M. Zuber, A. Nazir, M. Iqbal, M.I. Jilani, Photocatalytic degradation of disperse dye Violet-26 using TiO_2 and ZnO nanomaterials and process variable optimization, J. Mater. Res. Technol., 9 (2020) 1119–1128.
[26] R. Arshad, T.H. Bokhari, T. Javed, I.A. Bhatti, S. Rasheed, M. Iqbal, A. Nazir, S. Naz, M.I. Khan, M.K.K. Khosa, M. Iqbal, M. Zia-Ur-Rehman, Degradation product distribution of Reactive Red-147 dye treated by $UV/H_2O_2/TiO_2$ advanced oxidation process, J. Mater. Res. Technol., 9 (2020) 3168–3178.
[27] J.M. Rosa, E.B. Tambourgi, R.M. Vanalle, F.M. Carbajal Gamarra, J.C. Curvelo Santana, M.C. Araújo, Application of continuous H_2O_2/UV advanced oxidative process as an option to reduce the consumption of inputs, costs and environmental impacts of textile effluents, J. Cleaner Prod., 246 (2020) 119012, doi: 10.1016/j.jclepro.2019.119012.
[28] Z. Khan, O. Bashir, M.N. Khan, T.A. Khan, S.A. Al-Thabaiti, Cationic surfactant assisted morphology of Ag@Cu, and their catalytic reductive degradation of Rhodamine B, J. Mol. Liq., 248 (2017) 1096–1108.
[29] D. Hussain, M.F. Siddiqui, Z. Shirazi, T.A. Khan, Evaluation of adsorptive and photocatalytic degradation properties of $FeWO_4$/polypyrrole nanocomposite for rose bengal and alizarin red S from liquid phase: modeling of adsorption isotherms and kinetics data, Environ. Prog. Sustainable Energy, 41 (2022) 1–14.
[30] L.V. Dutra, C.R. de Oliveira Fontoura, J.C. da Cruz, M.A. Nascimento, A.F. de Oliveira, R.P. Lopes, Green synthesis optimization of graphene quantum dots by Doehlert design for dye photodegradation application, Colloids Surf., A, 651 (2022) 129442, doi: 10.1016/j.colsurfa.2022.129442.
[31] Z. Wang, H. Zhao, Y. Li, M. Yang, Z. Fang, Y. Zhang, Crystalline-dependent photocatalytic activity and exceptional dual selectivity of pyromellitic diimide for the photodegradation of dyes, Appl. Surf. Sci., 574 (2022) 151515, doi: 10.1016/j.apsusc.2021.151515.
[32] S. Rashmi, M. Michalska, M. Krajewski, K. Bochenek, A. Zaszczynska, T. Czeppe, L. Rogal, A. Jain, One-step synthesis of a sustainable carbon material for high performance supercapacitor and dye adsorption applications, Mater. Sci. Eng., B, 297 (2023) 116766, doi: 10.1016/j.mseb.2023.116766.
[33] S.J. Salih, A.S. Abdul Kareem, S.S. Anwer, Adsorption of anionic dyes from textile wastewater utilizing raw corncob, Heliyon, 8 (2022) e10092, doi: 10.1016/j.heliyon.2022.e10092.
[34] C. Nuanhchamnong, K. Kositkanawuth, N. Wantaneeyakul, Granular waterworks sludge-biochar composites: characterization and dye removal application, Results Eng., 14 (2022) 100451, doi: 10.1016/j.rineng.2022.100451.
[35] N. Oke, S. Mohan, Development of nanoporous textile sludge based adsorbent for the dye removal from industrial textile effluent, J. Hazard. Mater., 422 (2022) 126864, doi: 10.1016/j.jhazmat.2021.126864.
[36] G. Ravindiran, H. Sundaram, E.M. Rajendran, S. Ramasamy, A.-Z. Nabil, B. Ahmed, Removal of azo dyes from synthetic wastewater using biochar derived from sewage sludge to prevent groundwater contamination, Urban Clim., 49 (2023) 101502, doi: 10.1016/j.uclim.2023.101502.
[37] G. Vyavahare, P. Jadhav, J. Jadhav, R. Patil, C. Aware, D. Patil, A. Gophane, Y.H. Yang, R. Gurav, Strategies for crystal violet dye sorption on biochar derived from mango leaves and evaluation of residual dye toxicity, J. Cleaner Prod., 207 (2019) 296–305.
[38] B. Pieczykolan, P. Krzyżowska, Removal of Helaktyn Blue F-2R via adsorption onto modified post-coagulation sludge, Desal. Water Treat., 275 (2022) 103–115.
[39] B. Pieczykolan, I. Płonka, Post-coagulation sludge as an adsorbent of dyes from aqueous solutions, Ecol. Chem. Eng. S, 26 (2019) 509–520.
[40] B. Pieczykolan, I. Płonka, Application of excess activated sludge as waste sorbent for dyes removal from their aqueous solutions, Ecol. Chem. Eng. S, 26 (2019) 773–784.
[41] J. Babu, Z.V.P. Murthy, Treatment of textile dyes containing wastewaters with PES/PVA thin film composite nanofiltration membranes, Sep. Purif. Technol., 183 (2017) 66–72.
[42] M. Liu, Q. Chen, K. Lu, W. Huang, Z. Lü, C. Zhou, S. Yu, C. Gao, High efficient removal of dyes from aqueous solution through nanofiltration using diethanolamine-modified polyamide thin-film composite membrane, Sep. Purif. Technol., 173 (2017) 135–143.
[43] N. Gao, F. Liang, X. Wang, B. Li, Loose composite nanofiltration membrane with in-situ immobilized β-FeOOH film for effective dyes degradation and separation, Colloids Surf., A, 654 (2022) 130115, doi: 10.1016/j.colsurfa.2022.130115.
[44] Z. Sun, X. Zhu, F. Tan, W. Zhou, Y. Zhang, X. Luo, J. Xu, D. Wu, H. Liang, X. Cheng, Poly(vinyl alcohol)-based highly permeable TFC nanofiltration membranes for selective dye/salt separation, Desalination, 553 (2023) 116479, doi: 10.1016/j.desal.2023.116479.
[45] J. Yu, Y. He, Y. Wang, L. Zhang, R. Hou, Graphene oxide nanofiltration membrane for efficient dyes separation by hexagonal boron nitride nanosheets intercalation and polyethyleneimine surface modification, Colloids Surf., A, 656 (2023) 1–10.
[46] R. Rezaee, A. Faraji, F. Ashouri, Dendritic magnetic polymeric core-shell and cobalt-wastewater as an efficient peroxymonosulfate activator for degradation of tetracycline antibiotic and Methylene blue dye, Inorg. Chem. Commun., 146 (2022) 110184, doi: 10.1016/j.inoche.2022.110184.
[47] Í. Lacerda Fernandes, D. Pereira Barbosa, S. Botelho de Oliveira, V. Antônio da Silva, M. Henrique Sousa, M. Montero-Muñoz, J.A.H. Coaquira, Synthesis and characterization of the MNP@SiO_2@TiO_2 nanocomposite showing strong photocatalytic activity against Methylene blue dye, Appl. Surf. Sci., 580 (2022) 152195, doi: 10.1016/j.apsusc.2021.152195.
[48] P.O. Oladoye, T.O. Ajiboye, E.O. Omotola, O.J. Oyewola, Methylene blue dye: toxicity and potential elimination technology from wastewater, Results Eng., 16 (2022) 100678, doi: 10.1016/j.rineng.2022.100678.
[49] S. Yousefinia, M.R. Sohrabi, F. Motiee, M. Davallo, Enhanced simultaneous removal of Direct red 81 and bisphenol A from aqueous media by coupling nano zero-valent iron (nZVI) particles with graphene oxide and copper: isotherm and kinetic adsorption studies, Mater. Chem. Phys., 296 (2023) 127206, doi: 10.1016/j.matchemphys.2022.127206.
[50] S. Khamparia, D. Jaspal, Adsorptive removal of Direct red 81 dye from aqueous solution onto *Argemone mexicana*, Sustainable Environ. Res., 26 (2016) 117–123.
[51] M.M. Sahasrabudhe, R.G. Saratale, G.D. Saratale, G.R. Pathade, Decolorization and detoxification of sulfonated toxic diazo dye CI Direct red 81 by *Enterococcus faecalis* YZ 66, J. Environ. Health Sci. Eng., 12 (2014) 1–13.
[52] X. Yang, G. Xu, H. Yu, Removal of lead from aqueous solutions by ferric activated sludge-based adsorbent derived from biological sludge, Arabian J. Chem., 12 (2019) 4142–4149.

[53] T.S. Anirudhan, M. Ramachandran, Adsorptive removal of basic dyes from aqueous solutions by surfactant modified bentonite clay (organoclay): kinetic and competitive adsorption isotherm, Process Saf. Environ. Prot., 95 (2015) 215–225.
[54] T.M. Budnyak, S. Aminzadeh, I.V. Pylypchuk, D. Sternik, V.A. Tertykh, M.E. Lindström, O. Sevastyanova, Methylene blue dye sorption by hybrid materials from technical lignins, J. Environ. Chem. Eng., 6 (2018) 4997–5007.
[55] S. Sahu, S. Pahi, S. Tripathy, S.K. Singh, A. Behera, U.K. Sahu, R.K. Patel, Adsorption of Methylene blue on chemically modified lychee seed biochar: dynamic, equilibrium, and thermodynamic study, J. Mol. Liq., 315 (2020) 113743, doi: 10.1016/j.molliq.2020.113743.
[56] N. Fakhar, S.A. Khan, T.A. Khan, W.A. Siddiqi, Efficiency of iron modified *Pyrus pyrifolia* peels biochar as a novel adsorbent for Methylene blue dye abatement from aqueous phase: equilibrium and kinetic studies, Int. J. Phytorem., 24 (2022) 1173–1183.
[57] M. Dehghani, M. Ansari Shiri, S. Shahsavani, N. Shamsedini, M. Nozari, Removal of Direct red 81 dye from aqueous solution using neutral soil containing copper, Desal. Water Treat., 86 (2017) 213–220.
[58] T.A. Khan, S. Dahiya, I. Ali, Removal of Direct red 81 dye from aqueous solution by native and citric acid modified bamboo sawdust – kinetic study and equilibrium isotherm analyses, Gazi Univ. J. Sci., 25 (2012) 59–87.
[59] I. Khan, K. Saeed, I. Zekker, B. Zhang, A.H. Hendi, A. Ahmad, S. Ahmad, N. Zada, H. Ahmad, L.A. Shah, T. Shah, I. Khan, Review on Methylene blue: its properties, uses, toxicity and photodegradation, Water (Switzerland), 14 (2022) 242, doi: 10.3390/w14020242.
[60] Direct red 81, (n.d.).
[61] J. Blitz, Electrical and Magnetic Methods of Non-destructive Testing, NASA STI/Recon Tech. Rep. A, 94 (1991) 10775.
[62] S. Lagergren, Zur theorie der sogenannten adsorption geloster stoffe, K. Sven. Vetenskapsakademiens. Handl., 24 (1898) 1–39.
[63] Y.S. Ho, G. McKay, Pseudo-second order model for sorption processes, Process Biochem., 34 (1999) 451–465.
[64] M.J.D. Low, Kinetics of chemisorption of gases on solids, Chem. Rev., 60 (1960) 267–312.
[65] T. Ngulube, J.R. Gumbo, V. Masindi, A. Maity, Calcined magnesite as an adsorbent for cationic and anionic dyes: characterization, adsorption parameters, isotherms and kinetics study, Heliyon, 4 (2018) e00838, doi: 10.1016/j.heliyon.2018.e00838.
[66] O. Keskinkan, M.Z.L. Goksu, M. Basibuyuk, C.F. Forster, Heavy metal adsorption properties of a submerged aquatic plant (*Ceratophyllum demersum*), Bioresour. Technol., 92 (2004) 197–200.
[67] W.J. Weber, J.C. Morris, Kinetics of adsorption on carbon from solution, J. Sanit. Eng. Div., 89 (1963) 31–59.
[68] A.L. Prasad, T. Santhi, S. Manonmani, Recent developments in preparation of activated carbons by microwave: study of residual errors, Arabian J. Chem., 8 (2015) 343–354.
[69] H.M.F. Freundlich, Over the adsorption in solution, J. Phys. Chem, 57 (1906) 385–470.
[70] I. Langmuir, The adsorption of gases on plane surfaces of glass, mica and platinum, J. Am. Chem. Soc., 40 (1918) 1361–1403.
[71] D.S. Jovanovic, Physical adsorption of gases I: isotherms for monolayer and multilayer adsorption, Colloid Polym. Sci., 235 (1969) 1203–1214.
[72] M.M. Dubinin, L.V. Radushkevich, The equation of the characteristic curve of activated charcoal, Proc. Acad. Sci. Phys. Chem. Sect., 55 (1947) 331–337.
[73] R. Sips, On the structure of a catalyst surface, J. Chem. Phys., 16 (1948) 490–495.
[74] K. Björklund, L.Y. Li, Adsorption of organic stormwater pollutants onto activated carbon from sewage sludge, J. Environ. Manage., 197 (2017) 490–497.
[75] M.J. Martin, A. Artola, M.D. Balaguer, M. Rigola, Activated carbons developed from surplus sewage sludge for the removal of dyes from dilute aqueous solutions, Chem. Eng. J., 94 (2003) 231–239.
[76] E. Kacan, Optimum BET surface areas for activated carbon produced from textile sewage sludges and its application as dye removal, J. Environ. Manage., 166 (2016) 116–123.
[77] M. El Khomri, N. El Messaoudi, A. Dbik, S. Bentahar, A. Lacherai, Efficient adsorbent derived from *Argania spinosa* for the adsorption of cationic dye: kinetics, mechanism, isotherm and thermodynamic study, Surf. Interfaces, 20 (2020) 100601, doi: 10.1016/j.surfin.2020.100601.
[78] T.A. Khan, M. Nouman, D. Dua, S.A. Khan, S.S. Alharthi, Adsorptive scavenging of cationic dyes from aquatic phase by H_3PO_4 activated Indian jujube (*Ziziphus mauritiana*) seeds based activated carbon: isotherm, kinetics, and thermodynamic study, J. Saudi Chem. Soc., 26 (2022) 101417, doi: 10.1016/j.jscs.2021.101417.
[79] M. Saxena, N. Sharma, R. Saxena, Highly efficient and rapid removal of a toxic dye: adsorption kinetics, isotherm, and mechanism studies on functionalized multiwalled carbon nanotubes, Surf. Interfaces, 21 (2020) 100639, doi: 10.1016/j.surfin.2020.100639.
[80] Y. Wang, L. Hu, G. Zhang, T. Yan, L. Yan, Q. Wei, B. Du, Removal of Pb(II) and Methylene blue from aqueous solution by magnetic hydroxyapatite-immobilized oxidized multi-walled carbon nanotubes, J. Colloid Interface Sci., 494 (2017) 380–388.
[81] H. Zeng, K. Xu, F. Wang, S. Sun, D. Li, J. Zhang, Preparation of adsorbent based on water treatment residuals and chitosan by homogeneous method with freeze-drying and its As(V) removal performance, Int. J. Biol. Macromol., 184 (2021) 313–324.
[82] J.O. De Marques Neto, C.R. Bellato, J.L. Milagres, K.D. Pessoa, E.S. De Alvarenga, Preparation and evaluation of chitosan beads immobilized with iron(III) for the removal of As(III) and As(V) from water, J. Braz. Chem. Soc., 24 (2013) 121–132.
[83] S. Gamoudi, E. Srasra, Adsorption of organic dyes by $HDPy^+$-modified clay: effect of molecular structure on the adsorption, J. Mol. Struct., 1193 (2019) 522–531.
[84] L. Yan, L. Qin, H. Yu, S. Li, R. Shan, B. Du, Adsorption of acid dyes from aqueous solution by CTMAB modified bentonite: kinetic and isotherm modeling, J. Mol. Liq., 211 (2015) 1074–1081.
[85] S.I. Siddiqui, G. Rathi, S.A. Chaudhry, Acid washed black cumin seed powder preparation for adsorption of Methylene blue dye from aqueous solution: thermodynamic, kinetic and isotherm studies, J. Mol. Liq., 264 (2018) 275–284.
[86] M. Sh. Gohr, A.I. Abd-Elhamid, A.A. El-Shanshory, H.M.A. Soliman, Adsorption of cationic dyes onto chemically modified activated carbon: kinetics and thermodynamic study, J. Mol. Liq., 346 (2022) 118227, doi: 10.1016/j.molliq.2021.118227.
[87] M. Verma, P.K. Dwivedi, N.S. Saxena, Hollow silica nanoparticles synthesized from core-shell nanoparticles as highly efficient adsorbent for Methylene blue and its invitro release: mechanism and kinetics study, Colloids Surf., A, 587 (2020) 124333, doi: 10.1016/j.colsurfa.2019.124333.
[88] M. Arami, N.Y. Limaee, N.M. Mahmoodi, N.S. Tabrizi, Equilibrium and kinetics studies for the adsorption of direct and acid dyes from aqueous solution by soy meal hull, J. Hazard. Mater., 135 (2006) 171–179.
[89] Q. Gao, H. Zhu, W.J. Luo, S. Wang, C.G. Zhou, Preparation, characterization, and adsorption evaluation of chitosan-functionalized mesoporous composites, Microporous Mesoporous Mater., 193 (2014) 15–26.
[90] E.S. Dragan, D.F. Apopei Loghin, Enhanced sorption of Methylene blue from aqueous solutions by semi-IPN composite cryogels with anionically modified potato starch entrapped in PAAm matrix, Chem. Eng. J., 234 (2013) 211–222.
[91] L. Zhang, T. Xu, X. Liu, Y. Zhang, H. Jin, Adsorption behavior of multi-walled carbon nanotubes for the removal of olaquindox from aqueous solutions, J. Hazard. Mater., 197 (2011) 389–396.
[92] S. Lu, Z. Song, J. He, Diffusion-controlled protein adsorption in mesoporous silica, J. Phys. Chem. B, 115 (2011) 7744–7750.

[93] B.E. Wang, Y.Y. Hu, L. Xie, K. Peng, Biosorption behavior of azo dye by inactive CMC immobilized *Aspergillus fumigatus* beads, Bioresour. Technol., 99 (2008) 794–800.
[94] A. Özer, G. Akkaya, M. Turabik, The biosorption of Acid Red 337 and Acid Blue 324 on *Enteromorpha prolifera*: the application of non-linear regression analysis to dye biosorption, Chem. Eng. J., 112 (2005) 181–190.
[95] X. Wang, C. Jiang, B. Hou, Y. Wang, C. Hao, J. Wu, Carbon composite lignin-based adsorbents for the adsorption of dyes, Chemosphere, 206 (2018) 587–596.
[96] N. Can, B.C. Ömür, A. Altındal, Modeling of heavy metal ion adsorption isotherms onto metallophthalocyanine film, Sens. Actuators, B, 237 (2016) 953–961.
[97] I. Quiñones, G. Guiochon, Extension of a Jovanovic–Freundlich isotherm model to multicomponent adsorption on heterogeneous surfaces, J. Chromatogr. A, 796 (1998) 15–40.
[98] C.S.T. Araújo, I.L.S. Almeida, H.C. Rezende, S.M.L.O. Marcionilio, J.J.L. Léon, T.N. de Matos, Elucidation of mechanism involved in adsorption of Pb(II) onto lobeira fruit (*Solanum lycocarpum*) using Langmuir, Freundlich and Temkin isotherms, Microchem. J., 137 (2018) 348–354.
[99] M. Rahmayanti, A. Nurul Syakina, I. Fatimah, T. Sulistyaningsih, Green synthesis of magnetite nanoparticles using peel extract of jengkol (*Archidendron pauciflorum*) for Methylene blue adsorption from aqueous media, Chem. Phys. Lett., 803 (2022) 139834, doi: 10.1016/j.cplett.2022.139834.
[100] S. Li, L. Zhong, H. Wang, J. Li, H. Cheng, Q. Ma, Process optimization of polyphenol oxidase immobilization: isotherm, kinetic, thermodynamic and removal of phenolic compounds, Int. J. Biol. Macromol., 185 (2021) 792–803.
[101] S. Ullah, M.A. Bustam, A.G. Al-Sehemi, M.A. Assiri, F.A. Abdul Kareem, A. Mukhtar, M. Ayoub, G. Gonfa, Influence of post-synthetic graphene oxide (GO) functionalization on the selective CO_2/CH_4 adsorption behavior of MOF-200 at different temperatures; an experimental and adsorption isotherms study, Microporous Mesoporous Mater., 296 (2020) 110002, doi: 10.1016/j.micromeso.2020.110002.
[102] A. Sara-Maaria, E. Repo, E. Mäkilä, J. Salonen, E. Vakkilainen, M. Sillanpää, Adsorption behavior of hydrothermelly treated municipal sludge & pulp and paper industry sludge, Bioresour. Technol., 147 (2013) 71–76.
[103] A.O. Dada, A.P. Olalekan, A.M. Olatunya, O. DADA, Langmuir, Freundlich, Temkin and Dubinin–Radushkevich isotherms studies of equilibrium sorption of Zn^{2+} unto phosphoric acid modified rice husk, IOSR J. Appl. Chem., 3 (2012) 38–45.
[104] D. Ordonez, A. Valencia, H. Elhakiem, N. Bin Chang, M.P. Wanielista, Adsorption thermodynamics and kinetics of advanced green environmental media (AGEM) for nutrient removal and recovery in agricultural discharge and stormwater runoff, Environ. Pollut., 266 (2020) 115172, doi: 10.1016/j.envpol.2020.115172.
[105] M.J. Ahmed, S.K. Dhedan, Equilibrium isotherms and kinetics modeling of Methylene blue adsorption on agricultural wastes-based activated carbons, Fluid Phase Equilib., 317 (2012) 9–14.
[106] S.E. Rokni, R. Haji Seyed Mohammad Shirazi, M. Miralinaghi, E. Moniri, Efficient adsorption of anionic dyes onto magnetic graphene oxide coated with polyethylenimine: kinetic, isotherm, and thermodynamic studies, Res. Chem. Intermed., 46 (2020) 2247–2274.
[107] F. Kallel, F. Chaari, F. Bouaziz, F. Bettaieb, R. Ghorbel, S.E. Chaabouni, Sorption and desorption characteristics for the removal of a toxic dye, Methylene blue from aqueous solution by a low cost agricultural by-product, J. Mol. Liq., 219 (2016) 279–288.
[108] A.R. Tehrani-Bagha, H. Nikkar, N.M. Mahmoodi, M. Markazi, F.M. Menger, The sorption of cationic dyes onto kaolin: kinetic, isotherm and thermodynamic studies, Desalination, 266 (2011) 274–280.